

Creating 3D printed objects from scanning electron microscope images with photogrammetry

Yanick Samuel Bader

Dr. Jann Frey

Gymnasium Liestal

25.10.2023



Table of Contents

Abstract.....	4
1. Introduction	5
2. Theory.....	6
2.1 Scanning Electron Microscope.....	6
2.2 Structure from Motion Photogrammetry	8
2.3 3D-Printing	9
2.3.1 Material Extrusion.....	9
2.3.2 Light Polymerization.....	9
2.3.3 Powder Bed Printing	9
3. Methods	10
3.1 Acquisition of samples.....	10
3.1.1 Camera sensor	10
3.1.2 Drosophila melanogaster	10
3.1.3 Tartaric acid crystals	10
3.2 Preparation of samples	11
3.2.1 Dehydration (Only water containing samples)	11
3.2.2 Fixation on sample holder	12
3.2.3 Sputtering	12
3.3 Acquisition of images	12
3.3.1 Stage control, number, and angle of images.....	13
3.3.2 Maximizing depth of field.....	13
3.3.3 Resolution, noise levels, and contrast.....	13
3.4 Photogrammetry.....	15
3.5 Preparation of digital 3D models for 3D-printing	16
3.5.1 Clean-up of mesh	16
3.5.2 Simplification of mesh	16
3.5.3 Creating the printable model.	16
3.6 3D-Printing	17
3.6.1 Scaling and orienting.....	17
3.6.2 Support structures and printing	17
3.6.3 Post processing.....	18
4. Results	19
4.1 Edited and printed out models.....	19
4.2 Edited, but not printed out models	23
4.3 Not reconstructed models.....	25
5. Discussion.....	27
5.1 Quality and efficiency	27
6. Conclusion.....	29
7. Acknowledgements.....	30
8. Bibliography	31

Table of Figures

FIGURE 1 - FORMATION OF SECONDARY ELECTRONS (SE) AND BACKSCATTERED ELECTRONS (BSE) FROM PRIMARY ELECTRONS (PE).....	7
FIGURE 2 -INTERACTION VOLUME	7
FIGURE 3 - THE RAYLEIGH CRITERION IS MET IN THE MIDDLE.	8
FIGURE 4 -LENS ASSEMBLY	10
FIGURE 5 -GLASS.....	10
FIGURE 6 -CONTAINER	10
FIGURE 7 -PHASE TRANSITION DIAGRAM.....	11
FIGURE 8 -DRYING CHAMBER LID.....	11
FIGURE 9 -DROSOPHILA FLY ON SAMPLE HOLDER	12
FIGURE 10 -IMAGE QUALITY OF THE UNSPUTTERED (LEFT) AND SPUTTERED (RIGHT) CMOS SENSOR.....	12
FIGURE 11 -MANIPULATION OF STAGE AND THE EFFECT ON THE ELECTRON BEAM LOCATION.....	13
FIGURE 12 -EVENLY LIT (LEFT) AND UNEVENLY LIT (RIGHT) SUBJECT	14
FIGURE 13 -JOYSTICK AND KEYBOARD.....	14
FIGURE 14 -THE MODELS ON THE LEFT IN EACH IMAGE WERE RECONSTRUCTED USING AGISOFT METASHAPE WHILE MODELS ON THE RIGHT WERE RECONSTRUCTED USING ALICEVISION MESHROOM.	15
FIGURE 15 -POINT CLOUD OF DROSOPHILA MELANOGASTER IRREGULAR FACETS WITH CAMERA POSITIONS IN BLUE RECTANGLES.....	15
FIGURE 16 -THE PRINTABLE DROSOPHILA MELANOGASTER MODELS WITHOUT SUPPORT STRUCTURES.....	17
FIGURE 17 -THE PRINTABLE DROSOPHILA MELANOGASTER MODELS WITH SUPPORT STRUCTURES.	18
FIGURE 18 -BUILD PLATFORM	18
FIGURE 19 -DURING WASHING	18
FIGURE 20 -DURING CURING	18

Abbreviations

3D	Three-dimensional
BSE	Backscattered electrons
CMOS	Complementary metal-oxide semiconductor
FDM	Fused deposition modeling
SE	Secondary electron
SEM	Scanning electron microscope
SfM	Structure from motion
OLED	Organic light-emitting diode
SLS	Selective laser sintering
VP	Variable pressure
SLA	Stereolithography
DLP	Digital light processing
LCD	Liquid crystal display
CPU	Central processing unit
GPU	Graphic processing unit
RAM	Random-access memory
CT	Computerized tomography

Abstract

This paper explains how to obtain 3D printed models from scanning electron microscope (SEM) images with the help of the simple, affordable, and nondestructive 3D reconstruction method called photogrammetry. This method was evaluated on three test objects: a CMOS camera sensor, a regular drosophila fly, and a mutated drosophila fly.

To prepare water containing samples for high-vacuum conditions, CO₂ critical point drying was employed. All samples were sputtered with a 20 nm gold layer to prevent electrostatic charging and damage from the electron beam.

A Zeiss GeminiSEM 450 was used to capture the images. Depth of field was maximized using the microscope's depth of field setting, and the contrast was kept low to minimize overexposure and underexposure. To maximize the image coverage of the sample, as many images as possible were taken while rotating the stage 10° to 20° after every image until 360° were covered. The stage was then tilted 10° to 30°, depending on the sample. Image acquisition was limited by the stage's limited tilt range of -4° to +70°. The compucentric tilt and macro functions of the microscope were not working which made the acquisition of the images time intensive and difficult.

The SE2 (Everhart-Thornley) detector was used with appropriate acceleration voltage and current for each sample to acquire images with a resolution ranging from 12 to 30 megapixels, depending on the sample. Each picture was captured with an image cycle time of 1.5 minute and underwent “pixel average” noise reduction.

During the process, commercially available and open-source photogrammetry software, including Alicevision Meshroom, Agisoft Metashape, and OpenSFM were tested. Agisoft Metashape produced the best results in the shortest time, while Alicevision Meshroom and OpenSFM required extensive trial and error runs to achieve satisfactory results. Therefore, Agisoft Metashape was selected for use.

The raw digital models were repaired and simplified using Meshroom, Meshmixer and Blender. The digital models were then hollowed out to save resin and embedded into a stand to make them printable. Support structures were added to the digital models to enable printing. The models were printed with a light polymerization printer. Immediately after printing, the resin prints were washed with isopropanol and then cured under a 405 nm light at 70 degrees Celsius for 30 minutes. The support structures were removed from all samples, with the support structures of delicate parts being removed using tweezers, nail clippers, and razor blades.

This paper demonstrates that photogrammetry can be used to reconstruct 3D models from SEM images without special calibration. However, it is important to note that the accuracy of these models cannot be easily quantified, so they should not be used directly for quantitative measurements. For structures that are flat and simple and require accurate quantitative analysis, available stereophotogrammetry software solutions specifically designed for scanning electron microscopes are a better suited.

The results show that this method can produce high-quality 3D models with micron-scale resolution. This technique could be useful to create interactive models of samples with complex structures that could be used in areas like education and product development. Automated image acquisition makes this technique suitable for a professional environment.

Further research is required to investigate the effects of cycle time, image resolution, and number of overlapping images on quality of the models to improve the efficiency and quality of this method.

1. Introduction

Almost everyone has been exposed to photogrammetry, a range of techniques used to obtain three-dimensional information about physical objects from two-dimensional images (Aber, et al., 2010), e.g., through applications like Google Earth. After experiencing it through Google Earth, I was inspired to create 3D models using a camera drone and photogrammetry software. This fascination led me to other applications of photogrammetry, such as video game modeling, documenting cultural heritage, and mapping for geological surveys. Additionally, I was fascinated by the images produced by electron microscopes. When I had the unique opportunity to combine photogrammetry and electron microscopy, I began to consider ways to utilize the resulting models. With 3D printing as the last step, the idea of creating 3D printed models that could be used in education to better engage students with the subject through hands-on models, rather than two-dimensional images seemed good. The goal of this paper is to answer the following question: Wie erstellt man 3D gedruckte Modelle für den Naturwissenschaftsunterricht aus Aufnahmen eines Rasterelektronenmikroskop (REM)?

There are two common methods for non-destructive 3D model acquisition:

1. Surface 3D scanning

Surface 3D scanning is a broad term that encompasses a variety of techniques, such as LiDAR, time of flight, and structured-light scanning. These techniques all measure distances to the "camera" rather than recording color information, resulting in an "image" that serves as a documentation of the distances between points. Surface 3D scanning can be highly precise, but it is heavily dependent on surface properties such as reflectivity and translucence. (Wikipedia contributors, 2023).

2. Structure from motion (SfM) photogrammetry

Structure from motion (SfM) is a photogrammetric technique used to generate a point cloud from multiple photographs taken from different angles. It relies on the triangulation of corresponding features in the images to estimate distances between them (Aber, et al., 2010). SfM photogrammetry requires no specialized equipment other than a camera and the necessary software, making it a cost-effective option. However, it is dependent on favorable surface properties of the objects, even and adequate lighting, and a large depth of field. The resolution of SfM point clouds is generally lower than that of other techniques and can vary significantly depending on the equipment used and the object scanned. (Smith & Vericat, 2015).

Scanning electron microscopes (SEMs) record no information about depth. Therefore, 3D models must be obtained through photogrammetry. Some photogrammetry-based software for 3D reconstruction with scanning electron microscopes already exist, but they are limited in their ability to reconstruct complex objects like the ones presented in this paper. This is because they are primarily designed for analyzing features with limited topography through stereo photogrammetry (A.D., et al., 2017). It therefore seems that, with modern computers and advancements in SfM photogrammetry software, SfM photogrammetry from SEM images could, in some situations, serve as a viable alternative to dedicated laser scanning microscopes and existing stereo photogrammetry-based software.

SEMs are better suited for micro- to nanoscale photogrammetry than traditional light-based microscopes. This is because they have several unique characteristics: they are not affected by reflective or translucent materials, have an exceptionally large depth of field, and can image extremely small objects. Confocal light and laser microscopes can address some of these issues. However, scanning electron microscopes also have limitations: They do not capture color texture and are not suitable for imaging living or large objects. Additionally, many objects require extensive preparation for imaging, and the entire process can be time-consuming (Wikipedia contributors, 2023).

2. Theory

2.1 Scanning Electron Microscope

In contrast to traditional light microscopes, scanning electron microscopes (SEM) use a focused beam of electrons instead of light for high-resolution imaging. They operate by scanning an electron beam across the surface of a sample in a raster scan pattern. The electrons in the beam interact with the atoms in the sample and generate various signals. This sequential scanning with the electron probe, combined with the intensity of the detected signal, produces an image (Nanakoudis, 2019).

An SEM consists of the following main imaging components:

1. Electron gun

The electron gun usually consists of a tungsten filament or a field emission gun (which produces a more focused beam) that is heated to emit electrons. These electrons are typically accelerated to energies ranging from 0.5 keV to 30 keV.

2. Electromagnetic lenses

A series of electromagnetic lenses are used to determine the spot size, focus the image, and raster the beam. These electromagnetic lenses work by deflecting electrons through an electromagnetic field generated by coils carrying current. Electromagnetic lenses are used because electrons cannot pass through glass lenses.

3. Sample stage & Sample

The sample is mounted on the sample stage. The sample stage is used to control the position and orientation of the sample.

4. Detectors

Several detectors are used to detect various signals, including X-ray detectors, electron backscatter diffraction (EBSD) detectors, and others. Of particular importance for this work are:

- a) The Everhart-Thornley (secondary electron, SE) detector operates by using a scintillator that emits photons when struck by electrons. A positive but low voltage is used to selectively attract these electrons. High-energy electrons are not attracted enough to hit the scintillator unless their direction of travel is exactly right. Low-energy electrons are then accelerated onto the scintillator. (Goldstein, et al., 2018). This detector has low noise levels.
- b) Backscattered electrons (BSE) are detected by detectors that consist of semiconductor material. High-energy backscattered electrons directly strike the detector and generate a current. They are insensitive to the low-energy secondary electrons. These detectors are usually mounted above the sample (Luyk, 2019). This detector typically has higher noise levels than the Everhart-Thornley detector.

The stage is usually controlled through a joystick, and the image can be viewed on a screen.

The entire chamber of the electron microscope needs to be under a vacuum. This is because the interaction of the electron beam with air causes the electrons of the beam to scatter randomly, drastically reducing image quality. Therefore, samples must be suitable for a high-vacuum environment. Technologies like variable pressure (VP) and deep-cooled microscopy (Cryo-SEM) were developed to mitigate this problem but influence the image quality negatively. Due to the interaction of the samples with the electron beam, charging of nonconductive samples will inevitably occur. This can be resolved by coating nonconductive samples with a conductive material through a process called sputtering. The

VP mode also addresses this problem with ionized gas molecules that make the sample neutral without a conductive layer applied.

There are typically two types of signals carried by electrons resulting from their interaction (Figure 1) with the initial electron beam:

- Secondary electrons stem from inelastic collisions between the primary electron beam and the sample. They carry low energies (up to 50 eV) and are emitted from near the surface of the sample. This means that secondary electron images have high spatial resolution, making them ideal for imaging the surface topography of a sample (Nanakoudis, 2019).
- Backscattered electrons are electrons that are elastically scattered by the sample. They have higher energies than secondary electrons (ranging from 50 eV up to the incident beam energy) and can be emitted from deeper regions of the sample. This means that backscattered electron images have lower spatial resolution than secondary electron images. This signal can be used to identify separate phases of atoms in a sample, as the number of backscattered electrons is proportional to the atomic number (Nanakoudis, 2019).

The interactions that produce these signals occur in a teardrop shaped region within the sample, known as the interaction volume (Figure 2). The size of the interaction volume influences the spatial resolution of the image and depends on the acceleration voltage, the spot size, and the material properties of the sample (Nanakoudis, 2019).

There are several reasons why electron microscopes offer superior imaging capabilities compared to traditional light microscopes. One key factor is the wavelength of the illumination source, which directly determines the achievable resolution. Electrons have much shorter wavelengths compared to visible light, typically up to five orders of magnitude shorter (Wikipedia contributors, 2023).

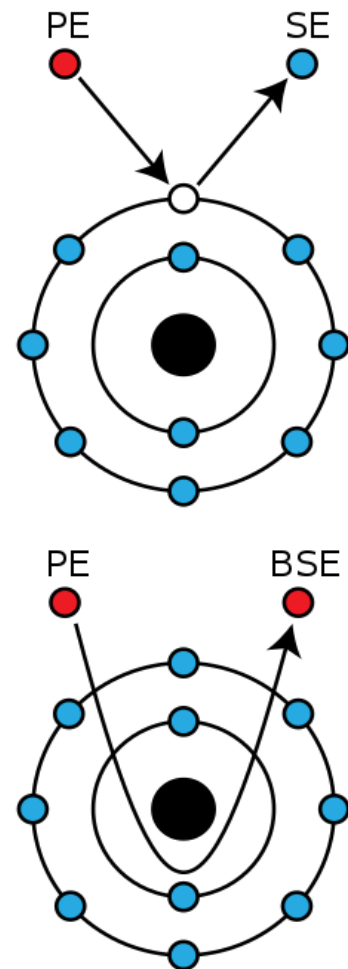


Figure 1 - Formation of secondary electrons (SE) and backscattered electrons (BSE) from primary electrons (PE) ⁽¹⁾

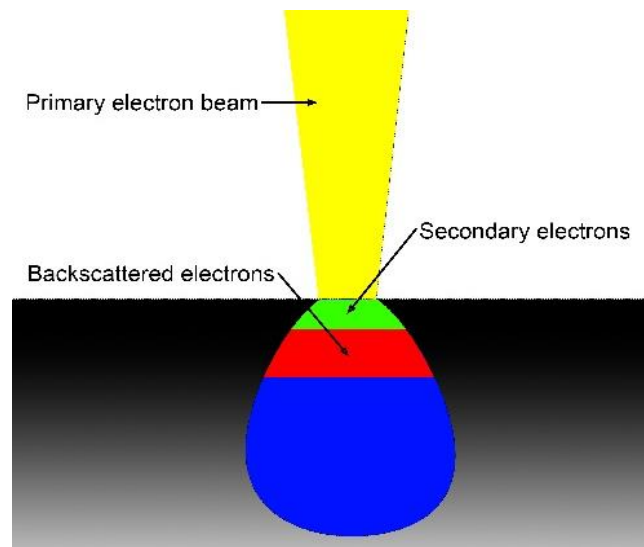


Figure 2 - Interaction volume

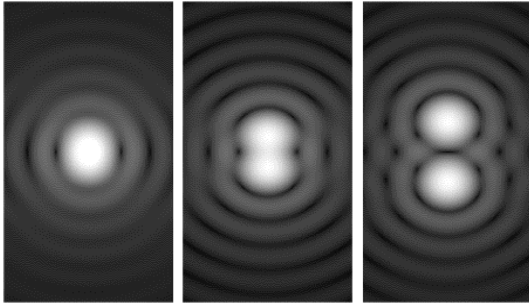


Figure 3 - The Rayleigh criterion is met in the middle. ⁽²⁾ (SamuelJ. Ling, 2016).

This is important because diffraction imposes a limit on resolution: The Rayleigh criterion is the minimum separation between two point-sources that can be resolved (see Figure 3). This criterion is directly dependent on the wavelength of the illumination source and the diameter of the aperture. It states that two point-sources are just resolvable when the first minimum of one diffraction pattern is directly over the second one

Electron microscopes are used in various fields of research, including materials science, biology, and medicine.

2.2 Structure from Motion Photogrammetry

Structure from motion photogrammetry (SfM) is a technique used to create 3D-Models from 2D-Images. The underlying principle is that multiple images from multiple viewpoints can be used to infer the 3D structure of the scene (Bolles, et al., 1987). It is like how humans perceive three-dimensional structures. When we move around, objects move a different amount depending on their distance to our eyes, which allows us to estimate their 3D structure.

SfM photogrammetry usually consists of the following steps:

1. Feature recognition and matching

The first step in SfM photography is to calibrate the camera and undistort the images. This is necessary to correct for lens distortion, which can cause significant errors during the reconstruction. Distortion, one of the most crucial lens characteristics, is usually measured using a test grid and computer software that calculates the distortion based on the camera and lens used. The next step is to extract unique and easily identifiable features from the images. Once these features have been extracted, they are matched across images by identifying corresponding features in different images that are likely to represent the same point in space (Micheletti, et al., 2015).

2. Structure estimation

After matching the corresponding features, the 3D structure is estimated, resulting in a point cloud that contains the coordinates of the matched features. The mathematical foundation of this process, although too complex to explain here, is based on the principles of collinearity (Nyimbili, et al., 2016).

3. Digital model generation

The generated point cloud is then meshed, creating continuous geometric shapes (Bern & Plassmann, 2000). This mesh can subsequently be textured, giving color information to the digital model.

Generally, any type of camera can be used for SfM photogrammetry, but higher-quality optics and sensors produce better images and carry less distortion and artifacts, which improves the quality of the results. Additionally, local motion signals such as satellite based positioning systems can be used to improve accuracy.

SfM photogrammetry is used in a wide variety of applications, including:

- Mapping terrains like riverbeds, badlands, and sandy coastlines (Javernick, et al., 2014) where traditional laser scanning methods (terrestrial and airborne) are too time consuming to use or are limited by the environment (Mancini, et al., 2013).
- Cheap and easy preservation of cultural heritage without the need for special equipment
- Character modelling for video games

2.3 3D-Printing

All 3D printers use the same underlying principle: They create 3D objects through additive processes, in contrast to traditional subtractive manufacturing methods such as milling and lathing, which remove material from an existing object. 3D printing is widely used: 3D printing is used in prototyping because it is fast, cost-effective and allows for rapid iteration compared to traditional methods. Some end-use products that come with complex geometries or low volume production runs are also being manufactured. Hobbyists use it for a lot of applications, including custom replacement parts and for art. There are three common techniques.

2.3.1 Material Extrusion

The most common technique is Fused Deposition Modeling (FDM). FDM printers melt a thermoplastic filament and deposit it onto the build platform. The thermoplastic cools and solidifies, creating a layer. This process repeats layer after layer. FDM printers are affordable and easy to work with but may lack the surface finish and accuracy of other methods (Shahrubudin, et al., 2019).

2.3.2 Light Polymerization

Stereolithography (SLA), Digital Light Processing (DLP), and liquid-crystal display (LCD) are three commonly used techniques. They function by using a photopolymer that polymerizes when exposed to light, typically ultraviolet light. In SLA printers, a laser traces the cross-section of the object on the surface of the liquid photopolymer, which then cures into a solid plastic. DLP and LCD resin printers operate on the same principle but expose an entire layer at a time instead of scanning the layer with a laser. LCD printers are popular among hobbyists and are more cost-effective. All these techniques enable high-resolution prints with a smooth surface finish. SLA printers achieve the highest quality but are also the most expensive among the three. Photopolymer printers are slower due to the time required for printing and post-processing. Caution is advised because photopolymers can cause allergic reactions. They are also generally more expensive (Shahrubudin, et al., 2019).

2.3.3 Powder Bed Printing

Powder bed printers, most commonly Selective Laser Sintering (SLS) printers, utilize a laser to sinter (melt) a powder into a solid structure. SLS printers are the most expensive on this list but produce strong and durable parts and allow for complex prints without requiring support structures, as is necessary with the other two methods (Shahrubudin, et al., 2019).

3. Methods

3.1 Acquisition of samples

A spirulina algae and a processor soldering point were used as proof of concept. They were already fully prepared for use in the microscope. These samples were used to initially evaluate whether this methodology works and to initially improve the workflow. They were not prepared for printing and printed. The *Drosophila melanogaster* samples were printed out, the camera sensor was prepared for printing but not printed out and the investigation with the crystal sample was discontinued.

3.1.1 Camera sensor

The 1/1.7-inch large main CMOS sensor was obtained from a Huawei P20 Pro. The camera sensor was removed from the lens assembly (see Figure 4) by pulling it from the connector until the glue gave way. It was then cleaned with acetone and ethanol to remove any glue residue. The connector was removed due to its large size. Note that the camera sensor sample was not printed. For more details see 6. Discussion.

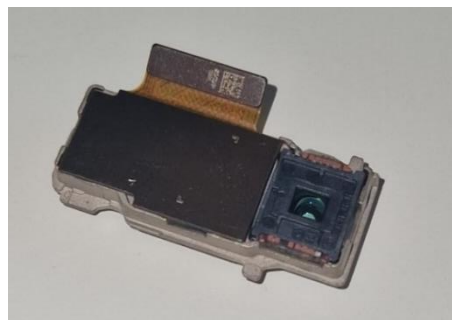


Figure 4 -Lens assembly

3.1.2 *Drosophila melanogaster*

Three mutant variants (yellow white, irregular facets, bar +) were stored alive in a glass with nutrition (Figure 5), which was closed with a Styrofoam plug. A hole was drilled into the Styrofoam plug, and a pipette containing chloroform was inserted. Chloroform was added dropwise, while taking care to ensure that no liquid chloroform was at the bottom of the glass, to prevent the flies from falling into it and damaging their tissues. After a few seconds, the flies ceased to move and eventually died. They were then transferred to containers suitable for the critical point dryer (Figure 6).



Figure 5 -Glass

3.1.3 Tartaric acid crystals

Tartaric acid is a chiral molecule, meaning that it has two enantiomers, which are mirror-image molecules of each other. The L-(+)-tartaric acid enantiomer is the more common form of tartaric acid found in nature. In this experiment, the goal was to recrystallize tartaric acid to produce the crystals that also act like mirror-images to each other. The L-(+)-tartaric acid enantiomer was selected for this experiment because it is more cost-effective.

The recrystallization was performed in 20 mL of deionized water at 70°C. 1.25 g of tartaric acid was dissolved into the water. A clean copper wire with a diameter of 2.5 mm² was suspended in the beaker. The beaker was covered and allowed to cool slowly overnight. The crystals that formed on the copper wire were removed with tweezers and stored in a paper towel for further use.



Figure 6 -Container

Note that the investigations using tartaric acid crystals were discontinued after imaging because it became evident that this material was not suitable for this project. For more details see 6. Discussion.

3.2 Preparation of samples

In scanning electron microscope (SEM) imaging, most samples require preparation to ensure high-quality results. Specific preparation steps are essential to make samples suitable for the high-vacuum environment of the SEM and to prevent charging artifacts (Dusevich, et al., 2010). The *Drosophila melanogaster*, camera sensor, processor and crystal samples were fully prepared following the steps in this section of the paper.

3.2.1 Dehydration (Only water containing samples)

The *Drosophila melanogaster* samples were dehydrated through critical point drying to prevent artifacts that could be formed due to the forces present when crossing a phase transition line. Critical point drying, marked in red (Figure 7) avoids the phase transition line by moving around the critical point, whereas traditional drying techniques, marked in green, cross the liquid-gaseous transition line and freeze drying, marked in blue, crosses the liquid-solid and solid-gaseous phase transition lines.

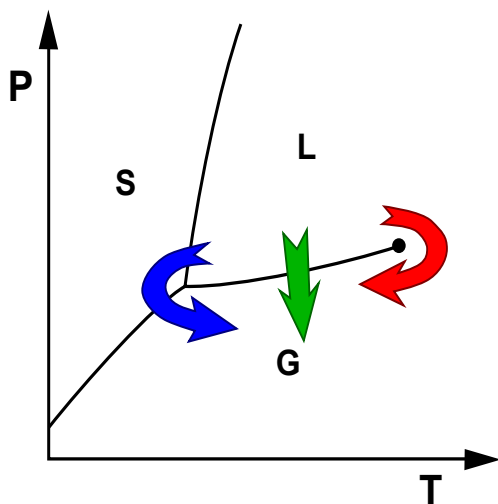


Figure 7 -Phase transition diagram ⁽⁴⁾



Figure 8 -Drying chamber lid

The following procedure was employed to dehydrate the samples:

1. The samples were initially fixed by immersing them in a 4% glutaraldehyde solution for 100 hours (Abay, et al., 2019).
2. The samples underwent two 5-minute submersions in a phosphate buffered saline solution, followed by a quick rinse with deionized water for 10 seconds.
3. To complete the dehydration process, the samples were immersed in a series of alcohol solutions with concentrations of 30%, 50%, 70%, 90%, and 100%, 10 minutes per step.
4. Critical point drying was performed, with CO₂ replacing the ethanol during this process, using a Tousimis Autosamdri 815 critical point dryer (Figure 8).
5. The critical point drying included 10 purge cycles within the device and took approximately 30 minutes to complete.

3.2.2 Fixation on sample holder

Drosophila melanogaster:

A hole with the exact diameter of a paperclip was drilled into the middle of a regular sample holder. Conductive silver glue was then used to glue the flies in an upright orientation. The paper clip was trimmed to 0.7 cm in length and glued into the drilled hole with conductive silver glue. This was done to allow for more of the sample to be visible in the microscope and to electrically connect the sample and sample holder (see Figure 9).



Figure 9 -Drosophila fly on sample holder

Other samples:

All other samples were attached to the sample holder with the help of precut double-sided tape. A bit of conductive silver glue was added to electrically connect the sample and sample holder.

3.2.3 Sputtering

To eliminate charging effects that negatively influence quality (Figure 10) and to prevent the samples from being altered by the high-energy electron beam, every sample was sputtered with a 20 nm thick layer of gold. The existing samples used for the proof of concept were resputtered if the existing gold layer showed signs of degradation. A Leica EM ACE600, a fully automatic sputtering machine was used.

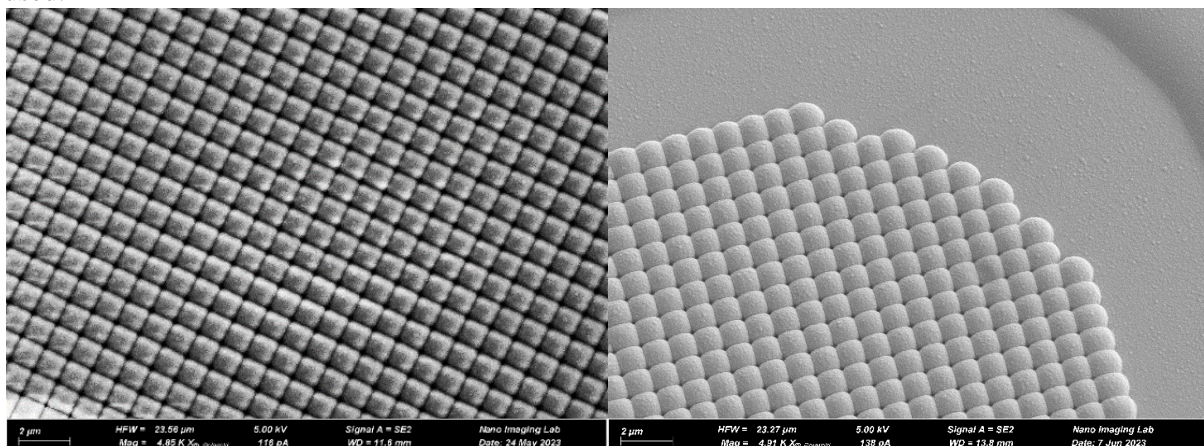


Figure 10 -Image quality of the unsputtered (left) and sputtered (right) CMOS sensor.

The samples were then stored in a plastic container until use to avoid contamination.

3.3 Acquisition of images

An acceleration voltage of 5kV was chosen for every sample, according to (Matusada, 2019) , and the microscope's auto current function was used to determine the optimal current setting.

Several factors contribute to the quality of the resulting 3D models in SfM photogrammetry, including a large depth of field, low noise levels, high resolution, and many overlapping images. Higher-quality images take longer to capture, so it is important to balance quality and speed. The used Zeiss GeminiSEM 450 provides many features that help to improve efficiency and quality.

3.3.1 Stage control, number, and angle of images

The scanning electron microscope (SEM) stage is limited in its movement. It can be moved in the X, Y, and Z directions, rotated 360 degrees, but can only be tilted in one axis. The SEM used in this study allows for a tilt between -4° and $+70^\circ$. Photogrammetry requires many images taken from different angles at regular intervals. This is extremely time-consuming to do by hand, as manipulating the stage inevitably results in a shift in the location of the electron beam, causing the image to shift and lose focus (Figure 11). The GeminiSEM is equipped with a compucentric stage feature that keeps the region of interest centered and in focus. However, this feature was not working during the acquisition of the images in this study. The GeminiSEM is also equipped with a macros function to automatically capture images and rotate the stage as required. However, due to the compucentric height feature not working, this feature was also unusable. Therefore, the stage was manually rotated 10° to 20° between images until 360° were covered. The stage was then tilted, and this process was repeated until all parts of the samples were covered, if possible.

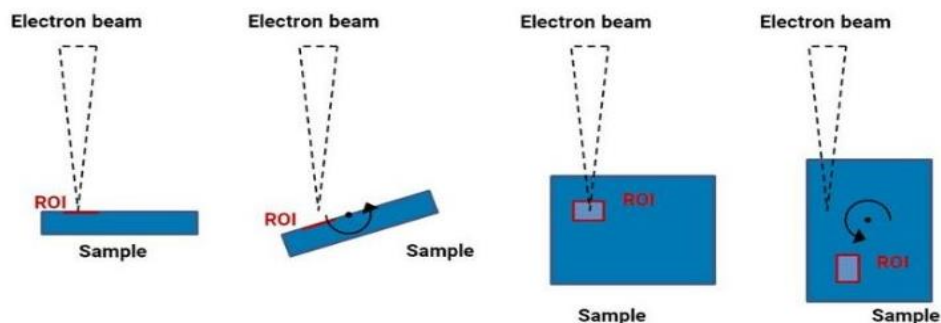


Figure 11 -Manipulation of stage and the effect on the electron beam location. ⁽⁴⁾

3.3.2 Maximizing depth of field.

Depth of field was maximized in two ways: The depth of field setting in the microscope was set to “100%” and the working distance was increased. The working distance is the distance between the subject and the electron column. Increasing the working distance increases the depth of field by decreasing the divergence of the electron beam, which increases the distance over which the beam remains focused (Luyk, 2020).

3.3.3 Resolution, noise levels, and contrast

High-resolution images are time-intensive to acquire, and balancing noise and resolution is a challenging task. The images of the camera sensor were shot at a resolution of 12MP, while the drosophila samples were captured at a resolution of 30MP due to their higher level of detail. A cycle time of 1.5 minutes was used per image, regardless of resolution, resulting in higher noise levels in the 30MP images. Longer cycle times would have reduced noise levels but also significantly extended the time required to capture the images. The “Pixel Avg.” noise reduction was used on all images. Even illumination on the sample is required for best reconstruction. As can be seen in Figure 12, the secondary electron Everhart-Thornley detector gives a strong directional illumination (A.D., et al., 2017). The BSD detector would have provided more even illumination but was not working as well as the SE2 detector due to its higher noise levels that require longer cycle times. The histogram function was used to keep the image from under and overexposing. This was done by reducing the contrast and adjusting the brightness of the image. The microscope captures the images at a bit depth of 8. To make the most of this bit depth, contrast has been maximized to the point where no clipping occurred.

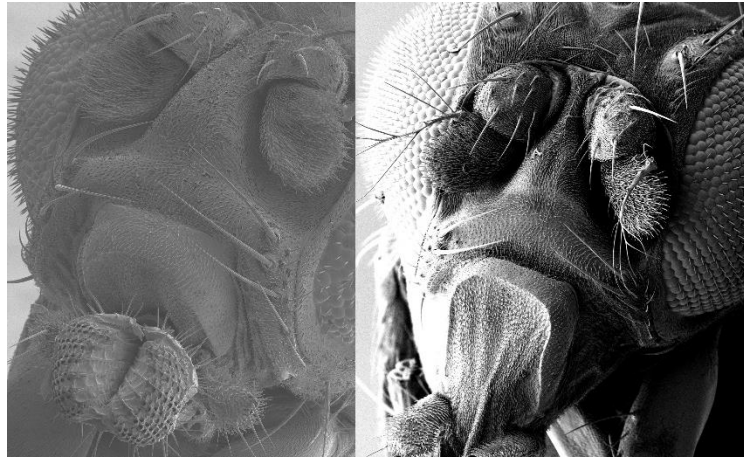


Figure 12 -Evenly lit (left) and unevenly lit (right) subject.

The equipment consisted of a monitor, a mouse, a joystick for stage control, and a keyboard with various knobs (Figure 13). For each sample, initial calibration of the electron beam was required. A high level of magnification was chosen, and the focus was set as accurately as possible initially. Subsequently, the beam was adjusted until no movement of the image was visible while moving the focal plane. This was achieved by using the "wobble" function, which shifted in and out of focus rapidly while adjusting the aperture X/Y knobs until no movement during the wobble was visible. This ensured that the beam was made parallel to the column. The astigmatism X/Y knobs were used to fine-tune the beam until no image blur, visible as stretching, was observed. This step ensured that the beam was made circular. If changes were made to the acceleration voltage, this procedure was repeated.



Figure 13 -Joystick and keyboard

The manual acquisition of the images was a very labor-intensive task due to the following challenges:

- Rotating the stage at high magnification took a long time because rotation speed decreases with magnification. This problem was solved by transitioning to a lower magnification setting, performing the stage rotation, and subsequently returning to a higher magnification.
- Turning the tilted and non-centered stage moved the object out of focus and out of frame. This was compensated for by moving the stage while rotating.
- Height readjustment was not accurately possible, which required refocusing after every turn.

All images were saved in .tif format with an 8-bit color depth. The image files were stored in a cloud-based storage solution provided by the University of Basel. Due to their large file size, initial data transfer was done using a USB stick, with cloud storage serving as a reliable backup solution.

3.4 Photogrammetry

Several photogrammetry software programs were evaluated, including VisualSFM, Alicevision Meshroom, and Agisoft Metashape (Standard). Alicevision Meshroom and Agisoft Metashape produced the best results, with Agisoft Metashape being faster, more reliable, and capable of generating higher-quality models (see Figure 14). However, Alicevision Meshroom required multiple trial-and-error runs to generate usable 3D models and had a longer overall runtime for each reconstruction step. VisualSFM was excluded from consideration due to its unreliability and inefficient performance. Ultimately, Agisoft Metashape (Standard) was selected for use after the proof-of-concept trial runs.

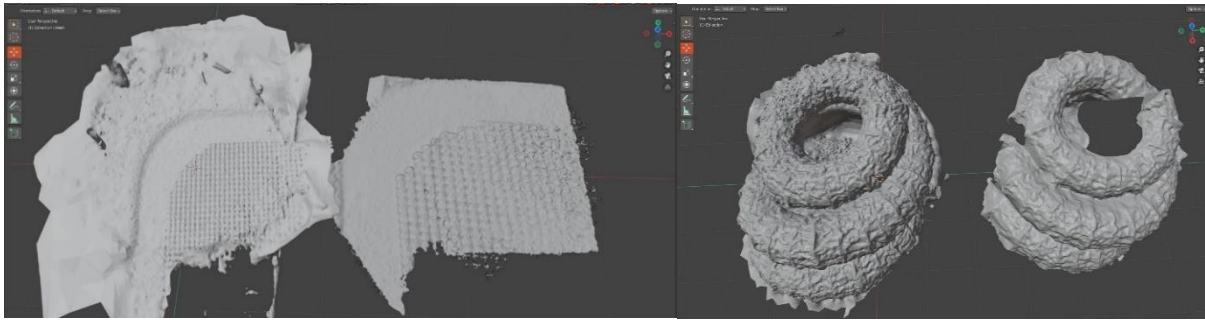


Figure 14 -The models on the left in each image were reconstructed using Agisoft Metashape while models on the right were reconstructed using Alicevision meshroom.

SfM photogrammetry typically necessitates information about camera intrinsics, particularly distortion, to accurately estimate spatial coordinates. Conventionally, this is achieved by using a calibration pattern to calculate the camera properties (Remondino & Fraser, 2006). However, this approach was unfeasible in this case as no calibration pattern was available for use in the microscope. Nonetheless, the results of the proof-of-concept samples were satisfactory.

The 3D models were reconstructed using Agisoft Metashape Professional Edition (version 1.9.1) on a computer with an Intel i7-9700K CPU, an AMD Radeon RX 5700-XT GPU, and 16GB of RAM.

The following steps were taken:

1. The images were imported into the software, and the "align photos" function was used to compute the point cloud model (Figure 15). The accuracy setting was set to "high" and the key point limit and tie point limit were set to "1,000,000" and "0", respectively. This sets the maximum number of extracted key points to 1,000,000 and uses every extracted point during reconstruction (Marcel, 2015). Depending on the number of images and extracted points, aligning the photos took between 30 and 60 minutes.

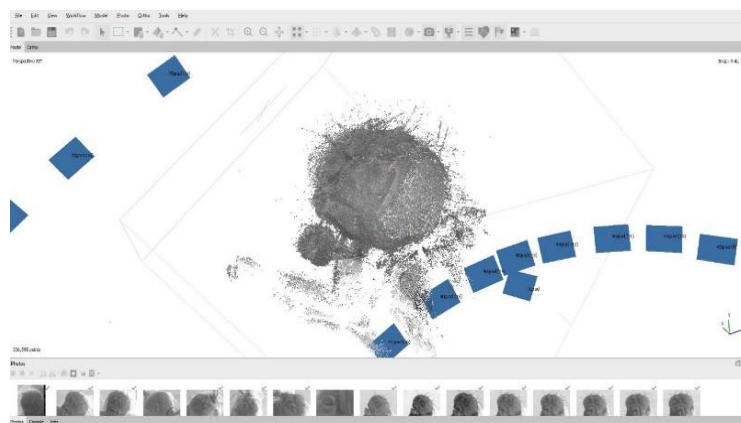


Figure 15 -Point cloud of *Drosophila melanogaster* irregular facets with camera positions in blue rectangles.

2. The "build mesh" function was used to generate a mesh from the previously created point cloud model. This step was executed with the "quality" setting set to "ultra-high" and the "face count" setting set to "high". This step took between 40 and 100 minutes, depending on the complexity of the model.
3. The texturization function was not used because the images were captured in grayscale and only the geometry of the models was needed for printing.
4. The digital models were then exported as .obj files.

3.5 Preparation of digital 3D models for 3D-printing

To prepare the digital 3D models for printing, they were edited in the open-source software Blender (version 3.4.1), MeshLab (version 2022.02) and Meshmixer (version 3.5.474).

The following steps were taken to make the models print ready:

3.5.1 Clean-up of mesh

MeshLab was used to remove non-manifold edges through the "Repair non-manifold edges" function. The models were then imported into Blender, where loose geometry was removed using the "Delete loose" function, and holes in the models were filled using the "Fill" function. The "Make planar faces" and "Dissolve degenerate" functions were used to ensure that all faces were planar and that there were no faces with zero area or edges with zero length. Further corrections were made automatically by the 3D printing software, as Blender's 3D printing tools caused problems with the models.

3.5.2 Simplification of mesh

Some of the digital models had large file sizes, which impacted the performance of Blender and made editing difficult. In Blender, the "Decimate" modifier was used to reduce the vertex and face count of the models, which directly reduced file size while retaining most of the geometry. The amount of decimation was determined through trial and error for each model. A ratio setting of 0.65 was a good balance between file size and the quality of the retained geometry. This means that 65% of the faces remained (Blender, 13). A ratio of 0.65 was used for the *Drosophila melanogaster* irregular facets and *Drosophila melanogaster* yellow white samples, while the geometry of the camera sensor was not decimated due to its smaller file size.

3.5.3 Creating the printable model.

Using Blender, the *Drosophila melanogaster* models were embedded in stands to make them suitable for display. The stands consisted of cylinders that were scaled and modified to fit the models. The stands were made hollow, and the name of the model and a scale bar were inserted as 3D text (Figure 16). The Boolean modifier, a mathematical operation that combines or subtracts two shapes to create a new shape was used to join all the models together. The modifier was applied to the cylinder while the photogrammetry models were used as the target of the modifier. It was set to the mode "union".

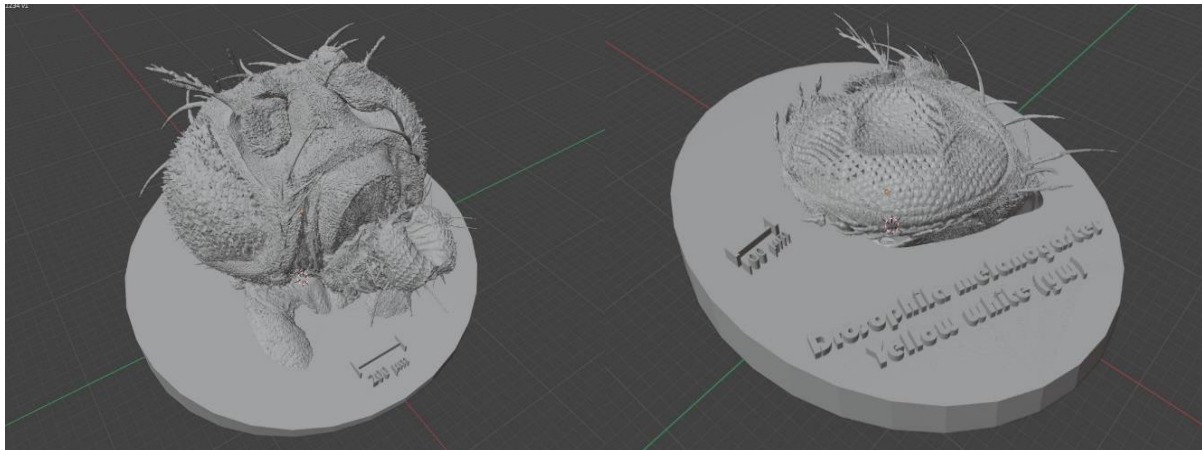


Figure 16 -The printable *Drosophila melanogaster* models without support structures.

The camera sensor model was prepared using Blender and Meshmixer. Unwanted parts and artifacts were removed in Blender. They were then imported into Meshmixer to add thickness to the models with the “solidify” modifier.

The models were then exported as .stl files for slicing in the printer software.

3.6 3D-Printing

A Formlabs Form 3B+ resin (SLA) printer was used to print the *Drosophila melanogaster* models. The *Drosophila melanogaster* yellow white model printed successfully on the first try, while the *Drosophila melanogaster* irregular facets model required two tries. The proprietary slicer software for Formlabs printers, PreForm, was used to prepare the resin prints. The models were imported into PreForm and the standard workflow was followed. The camera sensor model was not printed due to time limitations.

3.6.1 Scaling and orienting

Upon importing, the models were automatically repaired through Autodesk Fusion 360. The first step was to scale the models to their required size. The final model of *Drosophila melanogaster* yellow white was scaled to 40mm in x, 50mm in y, and 17mm in z. The final model of *Drosophila melanogaster* irregular facets was scaled to 90mm in x, 87mm in y, and 60mm in z. The models were then oriented using the “auto-orient” function.

3.6.2 Support structures and printing

All supports were manually placed because the automatic feature added an excessive number of touchpoints, which would have made removing the support structures challenging. Attempts to reduce the number of automatically generated touchpoints were unsuccessful as they were placed in inaccessible regions. The software highlighted inadequately supported parts of the structure in red. Fine, delicate structures were supported with the smallest possible touchpoint size of 0.25mm. These points were placed as far away from the body as possible to facilitate easier removal. Overhanging parts of the body that were not delicate were supported with a touchpoint size of 0.6mm. The brush tool was employed to cover the base with touchpoints sized at 0.7mm, using a spacing of 3mm and a brush radius of 5mm. The Raft Type setting was configured as Full Raft (see Figure 17). White v4 resin was used for the print, and the layer thickness was set to Adaptive. The resin supported a minimal layer thickness of 50 μ m, while the printer allows a minimal layer thickness of 25 μ m. This saved time during the printing process. An exact print duration for the *Drosophila melanogaster* yellow-white model cannot be provided since it was printed alongside other models. However, the *Drosophila melanogaster* irregular facets, which had a volume of 157ml, took 12 hours and 22 minutes to print out.

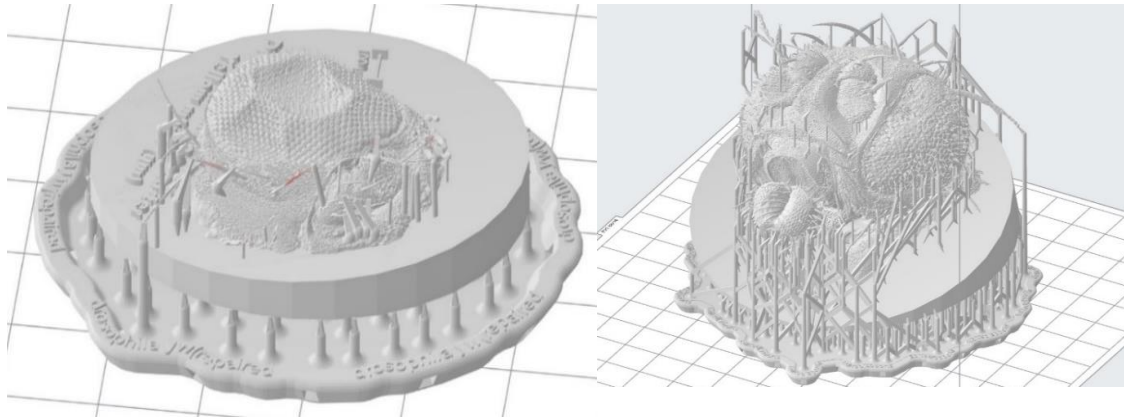


Figure 17 -The printable *Drosophila melanogaster* models with support structures.

3.6.3 Post processing

After printing, the models were processed as quickly as possible to avoid random unwanted polymerization. Nitrile gloves and goggles were worn during this process to avoid contact with the skin-irritating resin. The following steps were taken:

1. The prints were removed from the build platform using prying tools (Figure 18).
2. The prints underwent a thorough rinsing with isopropanol for 10 seconds, followed by a 10-minute manual wash in an isopropanol bath. This manual washing was performed to safeguard the delicate structures of the prints from potential damage by a washing machine (Figure 19). Subsequently, the prints were dried using compressed nitrogen.
3. The prints were cured under 405nm light at 70°C for 30 minutes (Figure 20).
4. The support structures were removed with the help of nail clippers, razor blades, and tweezers.
5. To ensure a level base, the prints' bases were smoothed using 150-grit sandpaper, with water applied to prevent the creation of harmful airborne dust. The models were washed with water and soap and then left to dry.
6. The *Drosophila melanogaster* Yellow white print was sputtered with a gold layer to enhance contrast.



Figure 18 -Build platform



Figure 19 -During washing

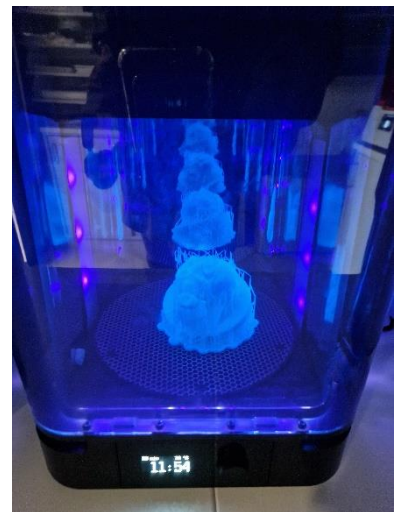


Figure 20 -During curing

4. Results

The scanning electron images are a compilation of the dataset acquired for reconstruction. The images of the unedited and edited 3D models were captured in MeshLab. The images of the ready to print 3D models were captured in Preform.

As mentioned in section 3.1, only *Drosophila melanogaster* was processed through all steps and printed out. Hence comprehensive results are provided for *Drosophila melanogaster* in section 4.1, while for the remaining objects partial results are provided in section 4.2 and section 4.3.

The following legend is applicable for the pictures presented in section 4.

- a) Light microscope images (with samples already sputtered)
- b) Scanning electron microscope (SEM) images
- c) Unedited 3D model
- d) Edited 3D model
- e) Ready to print 3D model.
- f) Printed, with support structures.
- g) Printed, without support structures.
- h) Printer, with gold coating.

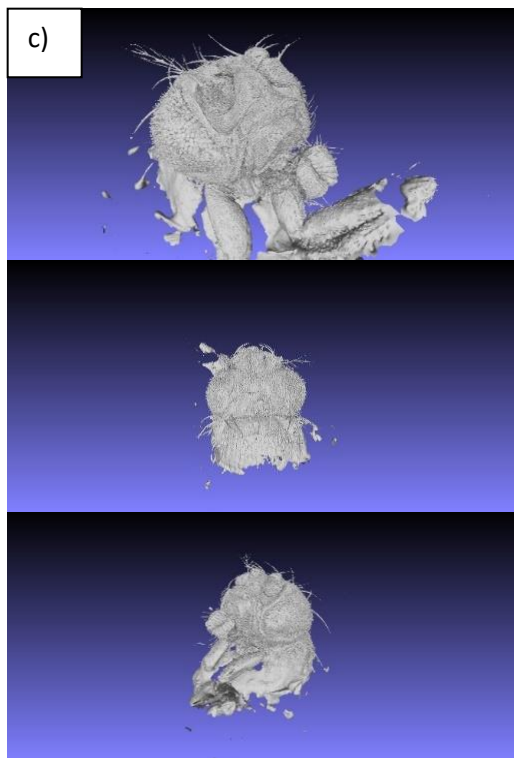
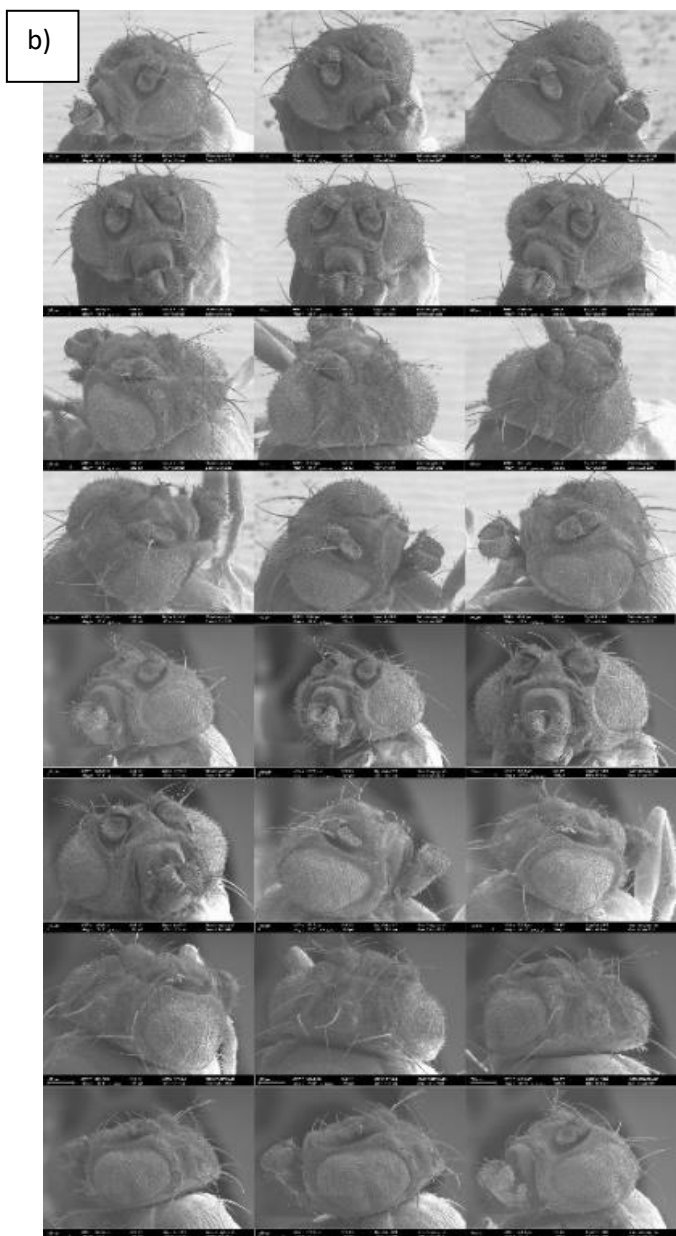
4.1 Edited and printed out models

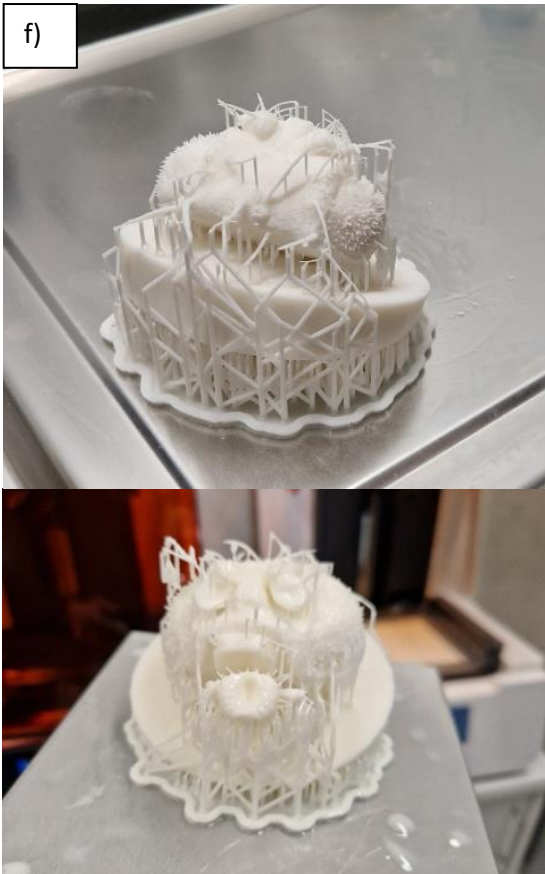
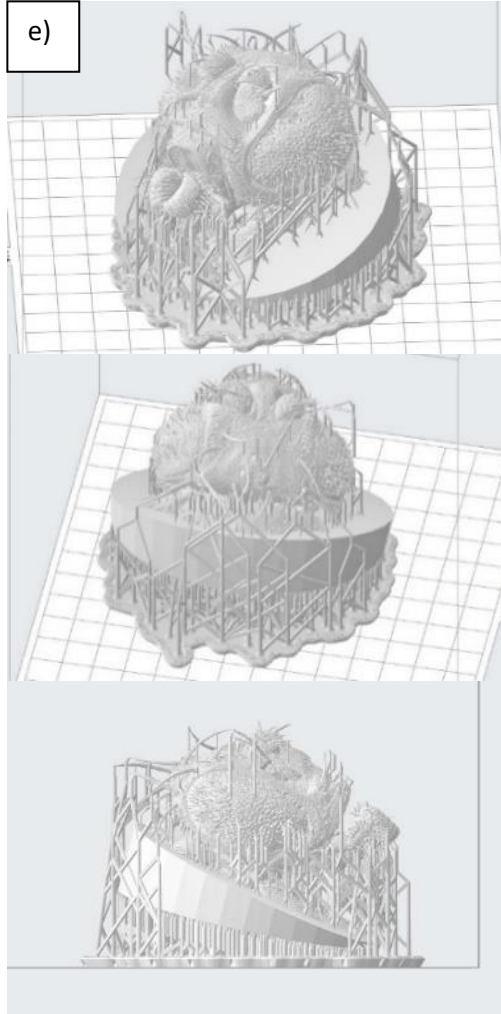
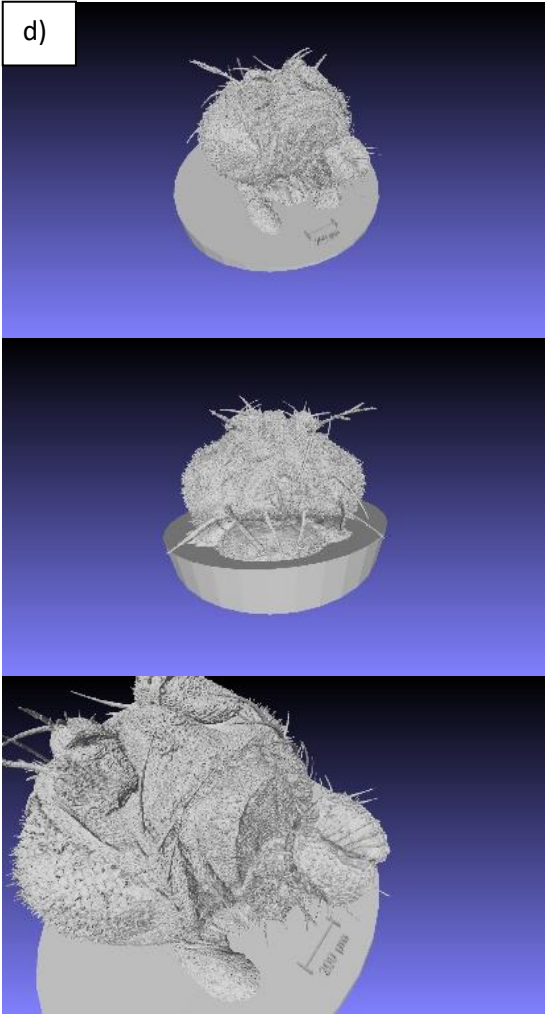
***Drosophila melanogaster*:** 10 flies were prepared per mutation. Out of this, the best-looking fly was selected. The *Drosophila melanogaster* irregular facets samples were successfully prepared while the *Drosophila melanogaster* yellow white samples had sunken eyes.

However, both samples were used as they were still considered to be suitable since the primary goal was to create 3D models and not to create authentic models.

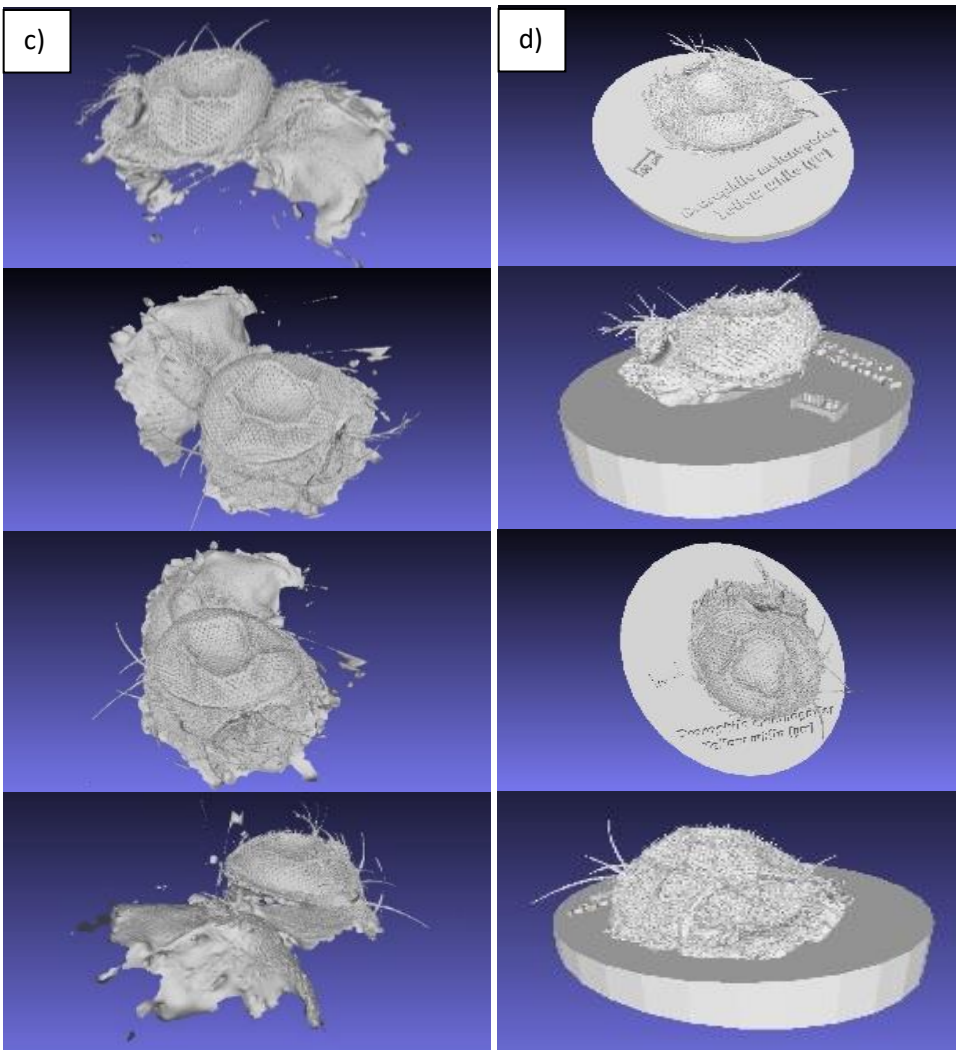
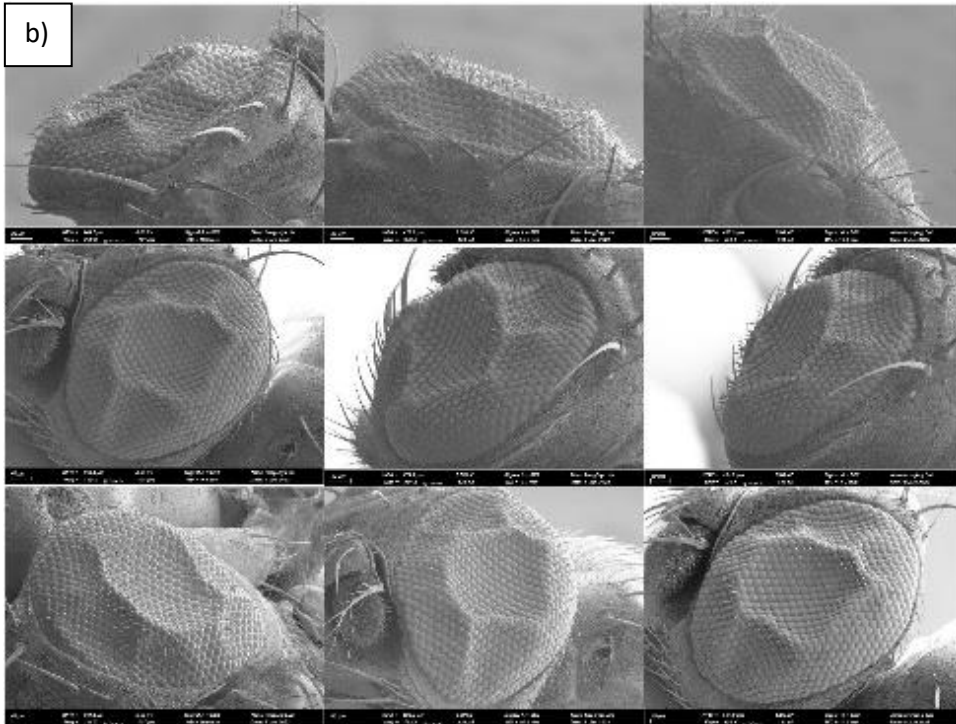
Only the *Drosophila* yellow white print was sputtered with a layer of gold as the *Drosophila* irregular facets print was too large to fit into the sputtering chamber.

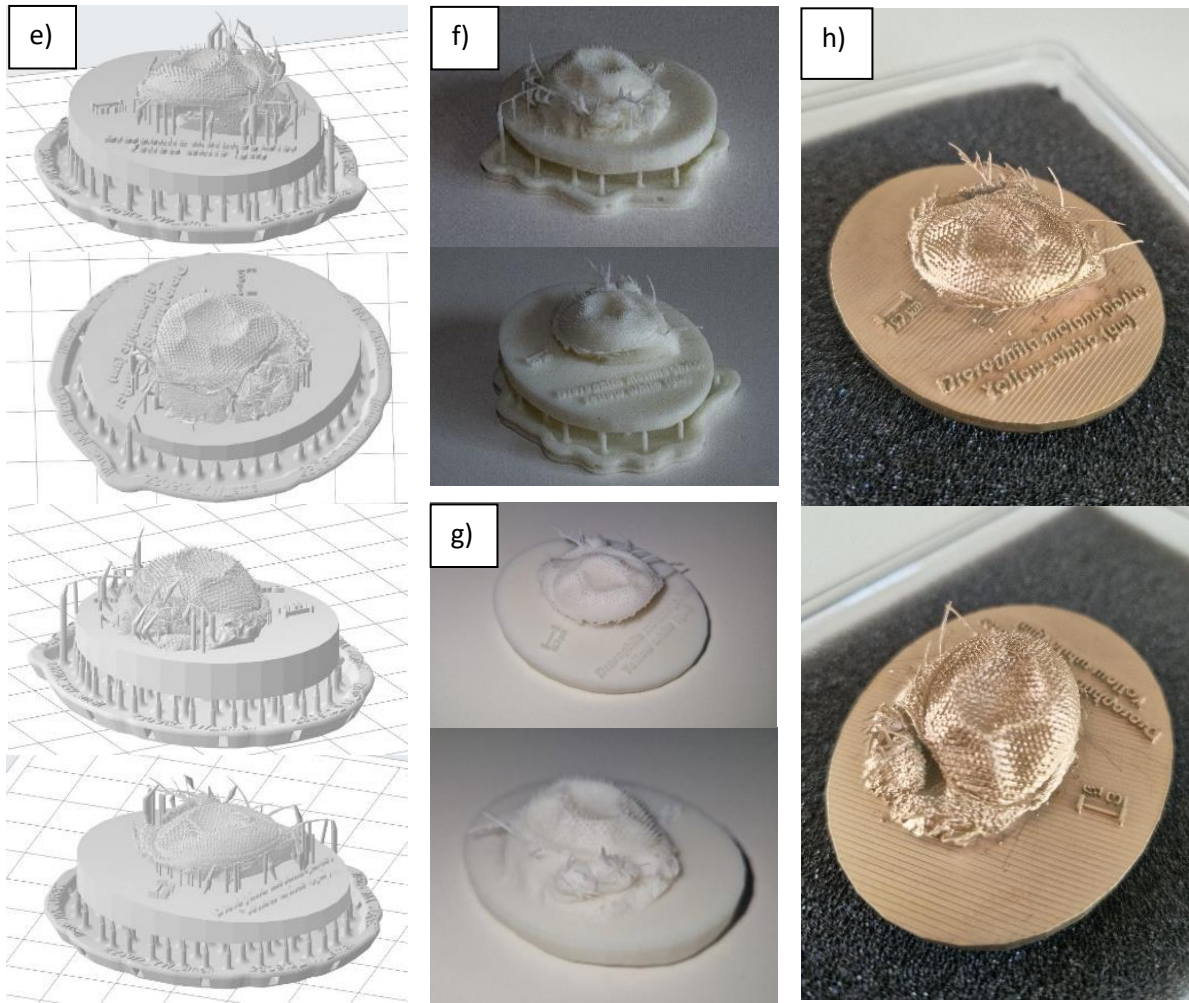
Drosophila melanogaster irregular facets:





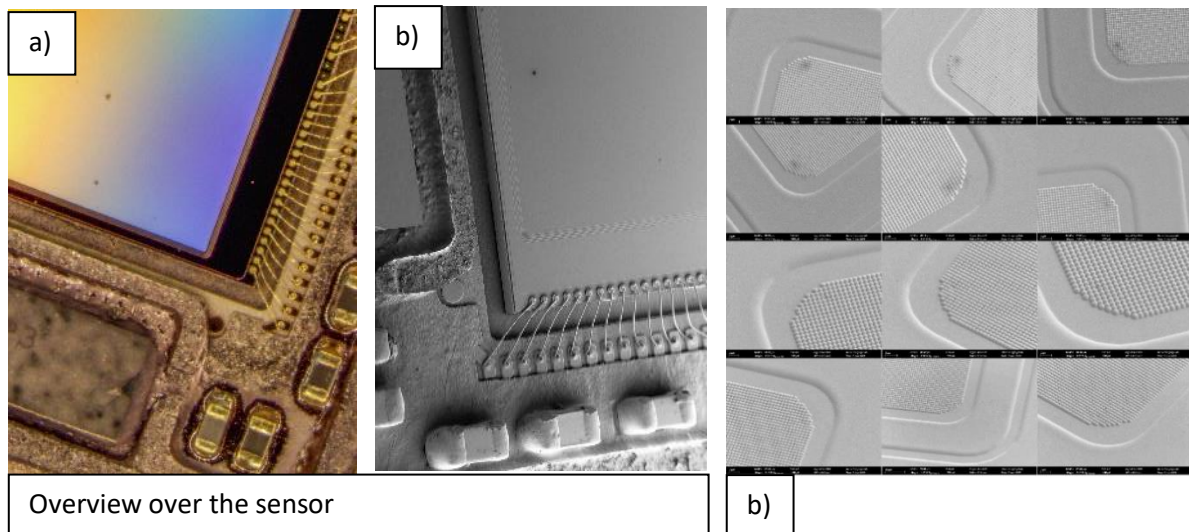
Drosophila melanogaster yellow white:





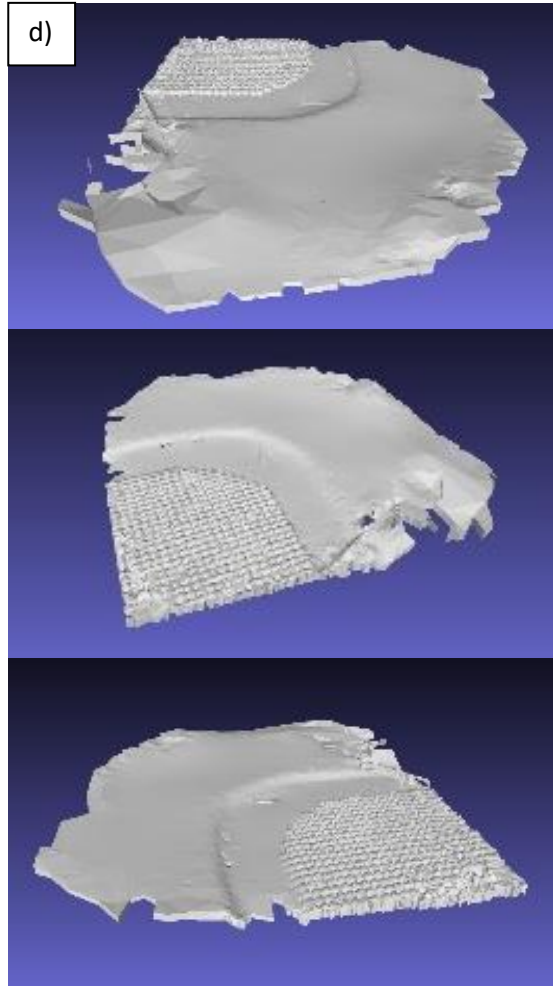
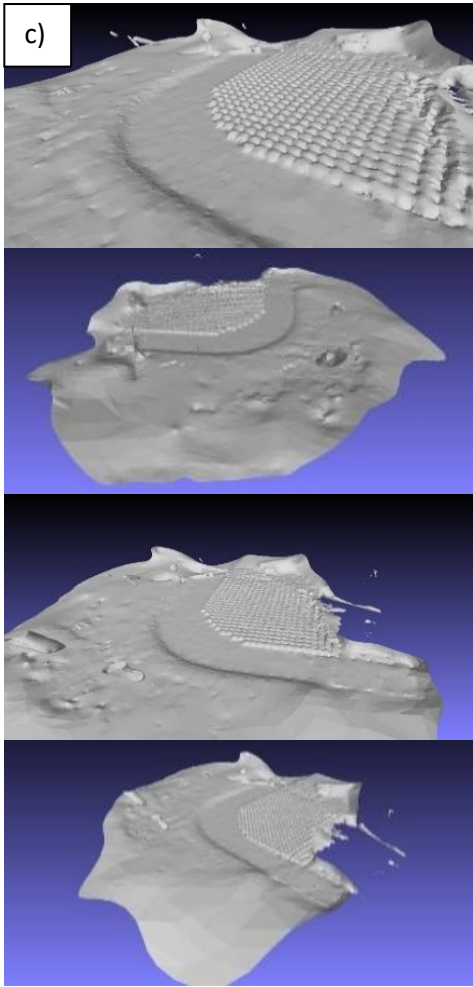
4.2 Edited, but not printed out models

Camera sensor (Not printed):

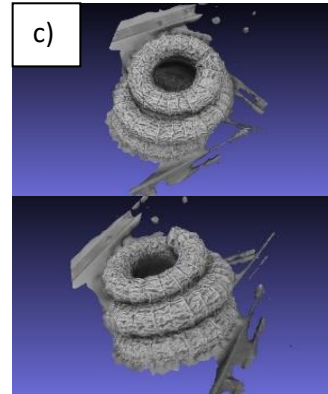
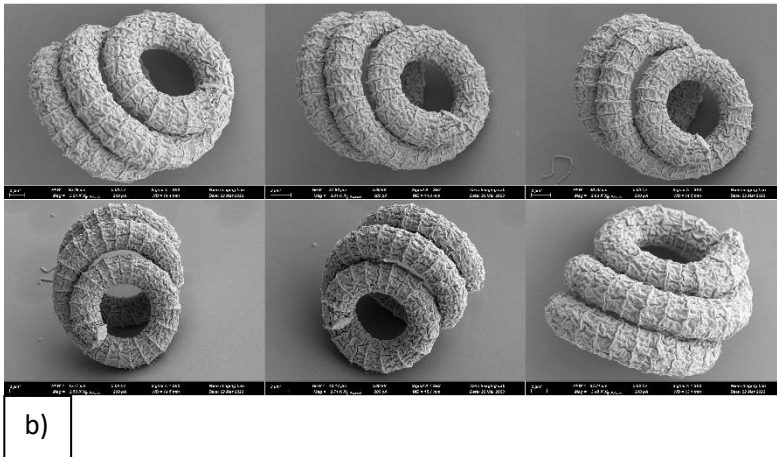


Overview over the sensor

b)



Spirulina algae (Proof of concept):



Miscellaneous:

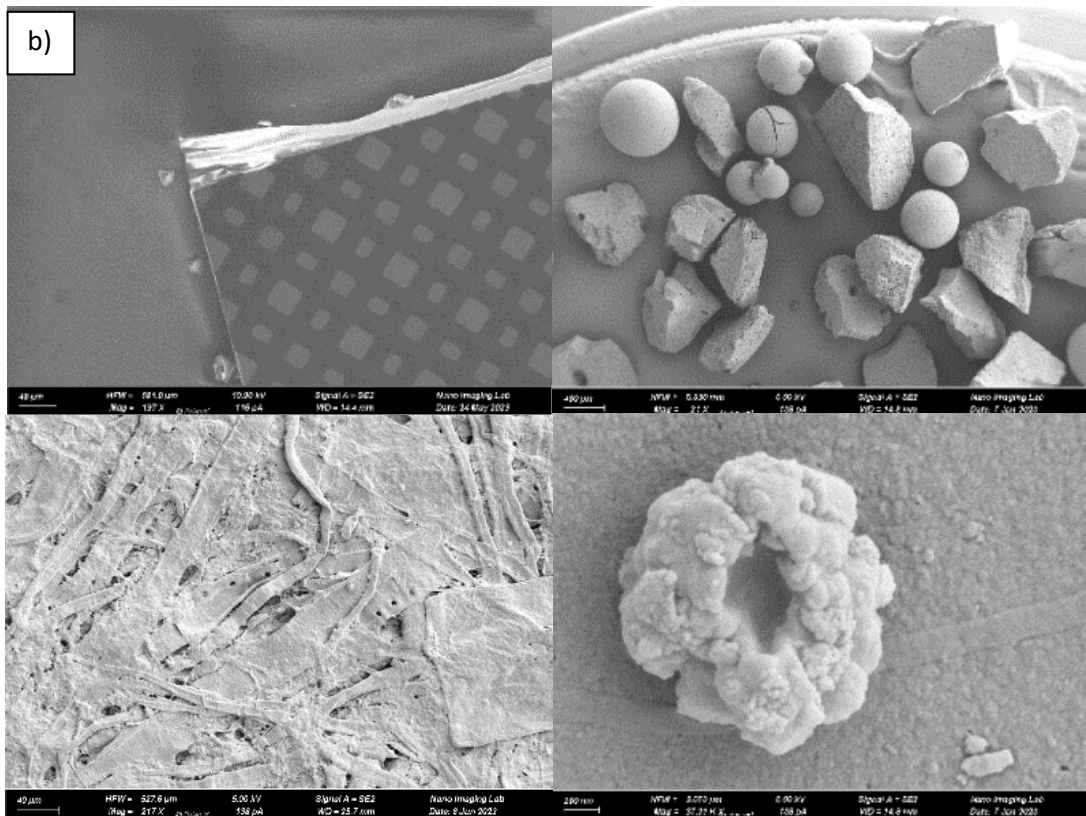
These images were taken during the search for suitable samples.

Top left: OLED Screen (Too flat and not interesting.)

Top right: Filter particles (Actually filtering structure would have been impossible to reconstruct because of the size compared to the particle.)

Bottom left: Paper (Would be interesting to test because of its topography but is not interesting as an educational model.)

Bottom right: Unknown particle



5. Discussion

Photogrammetry is an affordable and readily available technique for 3D reconstruction. This paper demonstrates that photogrammetry can be used to reconstruct 3D models from scanning electron microscope (SEM) images without special calibration. However, the accuracy of these models cannot be easily quantified, so they should not be used directly for quantitative measurements (see 5.1, Quality and efficiency). If the proportions of the model seem correct, distances can be approximated by using the scale bar in the scanning electron images to measure an easily and accurately identifiable distance and scaling the 3D model accordingly. For structures that are flat and simple and require accurate quantitative analysis, available stereophotogrammetry software solutions specifically designed for scanning electron microscopes are a viable alternative to this method.

During preparation, the *Drosophila melanogaster* yellow white sample was insufficiently fixated, resulting in a sunken eye. All other samples were successfully prepared.

One limiting factor of this method is the 5-axis SEM stage. As no 6-axis stage was available and the tilt was limited from -4° to $+70^{\circ}$, some areas of the sample were impossible to capture. To address this problem, some of the samples were mounted tilted on the sample holder, while others (*Drosophila melanogaster*) were raised above the sample holder to allow for more flexible mounting of the samples. This approach had the positive side effect of better separating the foreground from the background.

This technique could be useful for the visualization of models with complex structures, especially for researchers with limited access to specialized software and hardware. Automated image acquisition would be beneficial in a professional setting, as it would reduce the time needed to obtain 3D models and enable the reconstruction of larger and more detailed models with more images and angles.

3D printing of models with small and delicate parts proved to be a challenge. These models could only be printed on light polymerizing and powder bed printers, as extrusion printers struggle to print such complex objects with a high accuracy and appealing surface finish, especially when the size is limited (Mwema & Akinlabi, 2020). The cost of 3D printing on the Formlabs printer is very high due to the high resin costs. The printer itself is also very expensive (from 6500 CHF, 17.10.2023). Cheaper resin printers and cheaper resin is available but is very time consuming and can be messy to work with.

The camera sensor model was not printed due to time limitations. This model would have been interesting to print as it could be suitable for a regular extrusion printer (because of the larger size of its features) which would reduce print cost and time drastically.

5.1 Quality and efficiency

The quality of the models is hard to assess as no reference 3D scan is available. The proportions of the models were visually checked and seem to be all right. The accuracy of the models was not a priority to assess as the goal of this paper was to create visually appealing models.

These methods could be used to assess the accuracy:

- Using a reference 3D scan from a micro-CT or laser scanning microscope (if the properties of the sample allow it) allows for easy comparison of the proportions between the reference and photogrammetric reconstruction.
- Another method, inspired by (Kozikowski, 2020), is using a series of objects with simple geometry with known dimensions, performing photogrammetric reconstruction on them and measuring the dimensions of these objects in the 2D image (ideally captured at no tilt to minimize parallax effect) and comparing them to the relative size of the objects in the 3D model.

Sample preparation:

The crystal sample was found to be unsuitable as the lab grown and wine cork crystals only had slight resemblance to the characteristic tartaric acid crystals. The *Drosophila melanogaster* yellow white sample has a sunken eye because the tissue was not sufficiently fixed during preparation. The other *Drosophila melanogaster* sample was successfully prepared in the same batch, which is strange and needs further investigation. Repeating the experiment was not possible as the time didn't allow for it.

Image acquisition:

Image acquisition time was limited, preventing tests on the effect of image number and quality. An efficient and effective strategy was found to be capturing images at rotational angles of 20° and tilt angles ranging from 10° to 30°, yielding 50 to 90 images per sample. Effects of image resolution and noise on the outcomes could not be examined. For the *Drosophila melanogaster* sample, a resolution of 30 megapixels and cycle time of 1.5 minutes were chosen, mirroring contemporary cameras. However, this resolution was inadequate for reconstructing parts with denser and finer hairs. A higher resolution, albeit with longer cycle times, might have addressed this challenge, but would have inevitably extended acquisition duration. SfM photogrammetry often struggles with small and delicate structures (Beeler, et al., 2012). The images of the camera sensor had a resolution of 12 megapixels. This resolution was chosen to obtain lower noise levels with similar cycle times as the camera sensor had a very uniform surface. From experience with drone photogrammetry, uniform surfaces are extremely hard to reconstruct. Reducing noise levels was a higher priority than having a higher resolution, as this enabled the recognition of more "real" features instead of false features (noise). Still, the final model of the camera sensor was flawed through the false extraction and matching of features in the flat part of the sensor (where in reality no pixels are). Notably, the round pixels were well reconstructed. The phenomenon of flat surfaces negatively influencing the reconstruction was another reason to elevate the *Drosophila melanogaster* samples to have clear separation between the foreground and background.

Photogrammetry:

Round objects captured at high resolution and low noise levels achieved the best reconstruction results but required long cycle times and a large frame buffer. Calibration data and different software may also improve the results.

3D printing:

The quality of the 3D prints was excellent, but the base of the models (Raft) was insufficiently supported with touchpoints, requiring sanding after post processing to ensure a flat surface.

Efficiency:

This method is time-intensive, requiring several hours of sample preparation and image acquisition. Automated acquisition requires programming macros, while manual acquisition is easy but slow and prone to error. Manually acquiring images takes 1-5 hours per sample, or 2-4 minutes per image for an inexperienced user. Automated acquisition can be done overnight which makes this more viable. Programming the microscope through macros could be done fast if done by an experienced user. This requires a compucentric stage and macros function.

The photogrammetry process can be fully automated, reducing human interaction to a minimum. Reconstruction time depends on the computer's performance.

Making the models ready for 3D printing is time-intensive, with modeling and slicing taking several hours per model. Automated slicing can be done, but with the risk of failed prints or hard-to-remove support structures, which would extend post-processing time. Printing is time-intensive but can be done

overnight. Post-processing takes 30-120 minutes, depending on the amount and complexity of support structures and the need to remove resin residue. Powder bed printers are ideal, as they require no post-processing and can achieve similar precision. Regular extrusion printers can be a viable alternative for some models to reduce cost and post-processing time.

Acquiring unprocessed 3D models through photogrammetry is more time-intensive and gives worse results than comparable specialized methods like 3D laser scanning microscopy and Micro-CT, depending on the sample properties. The presented methodology has some special cases where it is the only method suitable, for example with very small objects requiring large magnification, special surface properties and more (Ball, et al., 2017).

6. Conclusion

The presented methodology is suitable for samples that are easy to prepare for high vacuum conditions with round features and no important small parts. Flat samples can be reconstructed using existing specialized stereophotogrammetry techniques for scanning electron microscopes.

These samples are well suited for this technique:

- Round objects, such as beads, spheres, and cylinders
- Objects with large features, such as fossils and insects
- Objects that are easy to prepare for high vacuum conditions.

Samples that are better suited for other techniques:

- Objects with flat surfaces, such as semiconductor wafers and printed circuit boards
- Objects that are difficult to prepare for high vacuum conditions.

Additional research is required to investigate the effect of cycle time, image resolution, and number of overlapping images on the result, to increase the efficiency and quality of this method. Older microscopes may struggle with this method, as they only support lower resolution images.

7. Acknowledgements

I am grateful to the Nano Imaging Lab of the Swiss Nanoscience Institute in Basel for their help and support throughout this project. I would especially like to thank Daniel Mathys from the Nano Imaging Lab for his guidance and assistance with the scanning electron microscope. I would also like to thank Dr. Ludovit Pavel Zweifel, head of the research instrumentation facility at the Biozentrum Basel, for his assistance and flexibility during the 3D printing process. Additionally, I would like to thank my supervisor, Dr. Jann Frey, for his guidance, advice, and ideas throughout the process.

I am also very grateful to the following people for their contributions to my research:

- Dr. Martin Müller for providing me with the *Drosophila melanogaster* flies and even giving me mutant variants of them.
- Dr. Marcus Wyss, head of the Nano Imaging Lab, for allowing me to work in the lab and for his support.
- Dr. Thilo Glatzel from the physics department for connecting me with the Nano Imaging Lab.
- Antoinette Stocker for providing me with all necessary chemicals, tools, and advice during the cleanup of the models and the growth of the crystals.
- Sonja Hindermann and Esther Lischer for their help with handling and storing the models.
- Susanne Erpel and Evi Bieler from the Nano Imaging Lab for discussing the first ideas with me and giving me more ideas.
- Dr. Silvia Bader-Weder for proofreading this work and supporting me through the whole process.

This work would have not been possible without the generous help of all these people.

Google Bard, based on PaLM 2, a factual language model from Google AI, was used for grammar and syntax correction. No text was directly copied and only recommendations were incorporated.

(arXiv preprint arXiv:2201.08237, 2022)

8. Bibliography

- A.D., B. A. L. L., P.A., J. O. B. & WALKER, A. E. L., 2017. SEM-microphotogrammetry, a new take on an old method for generating high-resolution 3D models from SEM images. *Journal of Microscopy*, Volume 267, pp. 214-226.
- Abay, A. et al., 2019. Glutaraldehyde – A Subtle Tool in the Investigation of Healthy and Pathologic Red Blood Cells. *Frontiers in Physiology*, Volume 10.
- Aber, J. S., Marzolff, I. & Ries, J. B., 2010. Chapter 3 - Photogrammetry. In: J. S. Aber, I. Marzolff & J. B. Ries, eds. *Small-Format Aerial Photography*. Amsterdam: Elsevier, pp. 23-39.
- Ball, A. D., Job, P. A. & Walker, A. E. L., 2017. SEM-microphotogrammetry, a new take on an old method for generating high-resolution 3D models from SEM images.. *Journal of microscopy*, August, 267(2), pp. 214-226.
- Beeler, T. et al., 2012. Coupled 3D Reconstruction of Sparse Facial Hair and Skin. *ACM Trans. Graph.*, July. Volume 31.
- Bern, M. W. & Plassmann, P. E., 2000. Mesh Generation.. *Handbook of computational geometry*, Volume 38.
- Blender, 13. *Blender Foundation*. [Online]
Available at: <https://docs.blender.org/manual/en/latest/modeling/modifiers/generate/decimate.html>
[Accessed 18 08 2023].
- Bolles, R. C., Baker, H. H. & Marimont, D. H., 1987. Epipolar-plane image analysis: An approach to determining structure from motion. *International Journal of Computer Vision*, Volume 1, p. 7–55.
- Dusevich, V. M., Purk, J. H. & Eick, J. D., 2010. Choosing the Right Accelerating Voltage for SEM (An Introduction for Beginners). *Microscopy Today*, January, Volume 18, pp. 48-52.
- Goldstein, J. et al., 2018. In: *Scanning electron microscopy and x-ray microanalysis*. Fourth edition ed. New(York): Springer New York, NY, pp. 115-116.
- Javernick, L., Brasington, J. & Caruso, B., 2014. Modeling the topography of shallow braided rivers using Structure-from-Motion photogrammetry. *Geomorphology*, Volume 213, pp. 166-182.
- Kozikowski, P., 2020. Extracting Three-dimensional Information from SEM Images by Means of Photogrammetry. *Micron*, Volume 134, p. 102873.
- Luyk, E., 2019. *Backscattered electrons in SEM imaging*. [Online]
Available at: <https://www.thermofisher.com/blog/materials/backscattered-electrons-in-sem-imaging/>
[Accessed 23 09 2023].
- Luyk, E., 2020. *Optimizing the Depth of Field in an SEM*, *ThermoFisher*. [Online]
Available at: <https://www.thermofisher.com/blog/materials/optimizing-the-depth-of-field-in-an-sem/>
[Accessed 05 09 2023].
- Mancini, F. et al., 2013. Using Unmanned Aerial Vehicles (UAV) for High-Resolution Reconstruction of Topography: The Structure from Motion Approach on Coastal Environments. *Remote Sensing*, Volume 5, p. 6880–6898.
- Marcel, 2015. *Agisoft Forum*. [Online]
Available at: <https://www.agisoft.com/forum/index.php?topic=3559.0>
[Accessed 24 07 2023].

- Matsusada, 2019. *Relationship between Acceleration Voltage and Image - Electron Microscope (SEM) Technical Explanation Series (1)*. [Online]
Available at: <https://www.matsusada.com/column/sem-tech1.html>
[Accessed 27 05 2023].
- Micheletti, N., Chandler, J. H. & Lane, S. N., 2015. *Structure from motion (SFM) photogrammetry*. s.l., s.n.
- Mwema, F. M. & Akinlabi, E. T., 2020. Basics of Fused Deposition Modelling (FDM). In: *Fused Deposition Modeling: Strategies for Quality Enhancement*. Cham: Springer International Publishing, p. 1–15.
- Nanakoudis, A., 2019. *SEM: Types of Electrons and the Information They Provide*. [Online]
Available at: <https://www.thermofisher.com/blog/materials/sem-signal-types-electrons-and-the-information-they-provide/>
[Accessed 18 09 2023].
- Nanakoudis, A., 2019. *What is SEM? Scanning Electron Microscopy Explained*. [Online]
Available at: <https://www.thermofisher.com/blog/materials/what-is-sem-scanning-electron-microscopy-explained/>
[Accessed 18 09 2023].
- Nyimbili, P. H., Demirel, H., Seker, D. Z. & Erden, T., 2016. *Structure from motion (sfm)-approaches and applications*. s.l., s.n., p. 27–30.
- Remondino, F. & Fraser, C., 2006. *Digital camera calibration methods. Considerations and comparisons*. Rio de Janeiro, ISPRS, pp. 266-272.
- SamuelJ. Ling, J. S. W. M., 2016. Double-Slit Diffraction. In: *University Physics Volume 3*. Houston, Texas: OpenStax, p. 163.
- Shahrubudin, N., Lee, T. C. & Ramlan, R., 2019. An Overview On 3d Printing Technology: Technological, Materials, And Applications. *Procedia Manufacturing*, Volume 35, pp. 1286-1296.
- Smith, M. W. & Vericat, D., 2015. From experimental plots to experimental landscapes: topography, erosion and deposition in sub-humid badlands from Structure-from-Motion photogrammetry. *Earth Surface Processes and Landforms*, Volume 40, pp. 1656-1671.
- Wikipedia contributors, 2023. *3D scanning*. [Online]
Available at: https://en.wikipedia.org/w/index.php?title=3D_scanning&oldid=1171517252
[Accessed 05 09 2023].
- Wikipedia contributors, 2023. *Electron microscope*. [Online]
Available at:
https://en.wikipedia.org/w/index.php?title=Special:CiteThisPage&page=Electron_microscope&id=1175340066&wpFormIdentifier=titleform
[Accessed 23 09 2023].

Image sources

All Images without an explicit source are by Yanick Bader, 2023. All scanning electron microscope images belong to the Nano Imaging Lab.

(1) By Rob Hurt - Own work, CC BY-SA 4.0,

<https://commons.wikimedia.org/w/index.php?curid=50931451>

(2) By Spencer Bliven - Own work, Public Domain,

<https://commons.wikimedia.org/w/index.php?curid=31456019>

(3) By Polyparadigm Image:Drying.PNG

<https://commons.wikimedia.org/w/index.php?curid=798711>

(4) By aryaao

<http://www.aryaao.com/en/cat/78-1/compucentric-stage.aspx>